The East Atlantic / West Russia teleconnection in the North Atlantic: climate impact and relation to Rossby wave propagation

Young-Kwon Lim

NASA Goddard Space Flight Center, Global Modeling and Assimilation Office,
Goddard Earth Sciences Technology and Research / I. M. System Group,
Greenbelt, Maryland, 20771, U.S.A.
Young-Kwon.Lim@nasa.gov

Submitted to Climate Dynamics
February 08, 2014

Abstract

Large-scale winter teleconnection of the East Atlantic / West Russia (EA/WR) over the Atlantic and surrounding regions is examined in order to quantify its impacts on temperature and precipitation and identify the physical mechanisms responsible for its existence. A rotated empirical orthogonal function (REOF) analysis of the upper-tropospheric monthly height field captures successfully the EA/WR pattern and its interannual variation, with the North Atlantic Oscillation as the first mode. EA/WR's climate impact extends from eastern North America to Eurasia. The positive (negative) EA/WR produces positive (negative) temperature anomalies over the eastern US, western Europe and Russia east of Caspian Sea, with negative (positive) anomalies over eastern Canada, eastern Europe including Ural Mountains and the Middle East. These anomalies are largely explained by lower-tropospheric temperature advections. Positive (negative) precipitation anomalies are found over the mid-latitude Atlantic and central Russia around ~60°E, where lower-level cyclonic (anticyclonic) circulation anomaly is dominant. The eastern Canada and the western Europe are characterized by negative (positive) precipitation anomalies.

The EA/WR is found to be closely associated with Rossby wave propagation. Wave activity fluxes show that it is strongly tied to large-scale stationary waves. Furthermore, a stationary wave model (SWM) forced with vorticity transients in the mid-latitude Atlantic (~40°N) or diabatic heat source over the subtropical Atlantic near the Caribbean Sea produces well-organized EA/WR-like wave patterns, respectively. Sensitivity tests with the SWM indicate improvement in the simulation of the EA/WR when the mean state is modified to have a positive NAO component that enhances upper-level westerlies between 40-60°N.

1. **Introduction**

Large-scale teleconnection patterns that persist from days to months are known to play an important role in determining whether a particular season will be warm or cold, wet or dry. The teleconnection patterns, often defined in terms of the height and/or sea level pressure fields, and the corresponding atmospheric circulation fields typically cover vast geographical areas (Barnston and Livezey 1987).

The North Atlantic Oscillation (NAO) is one of the primary modes of atmospheric variation over the North Atlantic, impacting seasonal climates over North America and Europe (e.g., Hurrell 1995; Donat et al. 2010; Sugimoto and Hanawa 2010). Other teleconnection patterns with an important component in the North Atlantic region are the Scandinavia (SCA) (Wallace and Gutzler 1981; Bueh and Nakamura 2007), the East-Atlantic (EA) (Washington et al. 2000; Bojariu and Reverdin 2002), and the East Atlantic / West Russia (EA/WR) (Barnston and Livezey 1987; Washington et al. 2000; Wang et al. 2011) patterns. While numerous earlier studies investigated the NAO because of its dominant large-scale influences on climate variability, impact of the other teleconnections on climate variability over the North Atlantic and generation of their patterns have yet to be addressed in more detail. Particularly, the EA/WR, which is characterized by two main large-scale anomalies located over the Caspian Sea and western Europe, has not attracted any significant and detailed investigation despite the recognition of EA/WR as one of the leading teleconnections over the North Atlantic (Barnston and Livezey 1987; Washington et al. 2000). Wang et al. (2011) and Lim and Kim (2013) suggested that understanding EA/WR is very important because not only its impact extends across the European mainland, but also the impact reaches mid-latitude East Asia as a planetary-

64 scale stationary wave pattern. The possible role of EA/WR in modulating the east Asian winter
65 monsoon variability was analyzed by Wang et al. (2011) and Kim et al. (2013).

66 Regarding the interrelationship among the teleconnections over the Atlantic, Scherrer et al.
67 (2006) investigated the possible relationship between the NAO and large-scale atmospheric
68 blocking located over the Atlantic, the Scandinavian Peninsula, and mainland Europe.
69 Specifically, the study identified that a change in the intensity of the westerlies over the central
70 latitudes of the eastern North Atlantic and over much of Europe associated with the NAO, is at
71 times associated with a long-lived atmospheric blocking in the vicinity of Great Britain and the
72 Scandinavian Peninsula. Pavan et al. (2000) and Shabbar et al. (2001) addressed that atmospheric
73 blocking over the North Atlantic seems more frequently observed during a substantial negative
74 NAO. However, there are some indications that blocking-like persistent high-pressure systems
75 over the European mainland are more related to the positive NAO phase (Wanner et al. 2001).
76 Overall, it appears that there is still much to be learned about possible inter-relationships
77 between the various modes, including the potential role of other key large-scale patterns (e.g.,
78 ENSO) in modulating teleconnection patterns in this region.

79 Turning to the physical mechanisms responsible for these patterns of variability, there is
80 some evidence for an important role of wave propagation forced by transient eddies. Bueh and
81 Nakamura (2007) found that transient eddies migrating along the storm track together with
82 incoming Rossby wave activity from the Atlantic are crucial for maintaining teleconnection
83 pattern. Several other studies also argued that heating over the Atlantic may be responsible for
84 producing the atmospheric teleconnection (e.g., Walter et al. 2001; Wang et al. 2011). Clearly,
85 the relative importance of heating and weather transients, and the primary source regions for
86 generating Rossby waves associated with the various Atlantic teleconnections needs clarification.

87 The purpose of this study is to provide a better (physically-based) understanding of the
88 impacts of the EA/WR teleconnection on winter climate over the North Atlantic and surrounding
89 regions, and their relation to Rossby wave propagation. This study takes advantage of the latest
90 high-resolution (~0.5° latitude/longitude) reanalysis data to document the impacts of the EA/WR
91 pattern on temperature and precipitation over the Arctic, western Russia, eastern North America,
92 North Africa and Europe. The stationary wave model of Ting and Yu (1998) is used to examine
93 the role of stationary Rossby waves in explaining the structure and forcing of these patterns.
94 Section 2 describes the data and stationary wave model utilized in this study. The capture of
95 the EA/WR spatial pattern and its interannual variation over the study domain is described in
96 Section 3. Section 3 also discusses the atmospheric circulation and other features associated
97 with the EA/WR that acts to produce the regional climate impacts. Section 4 identifies the source
98 regions and the propagation of large-scale stationary waves associated with the EA/WR pattern,
99 and includes an assessment of the sensitivity of the response to the basic state tied to variations
100 in the NAO or ENSO. This is followed by the concluding remarks in Section 5.
101
102 **2. Data and Model**
103 This study uses the Modern-Era Retrospective analysis for Research and Applications
104 (MERRA) reanalysis data (Rienecker et al. 2011) to analyze the past 33 winters (December,
105 January, February or DJF) from 1979/80 through 2011/12. The key variables consist of SST,
106 upper-level (250hPa and 300hPa) geopotential height, wind (300hPa and 850hPa), temperature
107 (300hPa, 850hPa, and 2 meter level), sea level pressure (SLP), diabatic heating (residually
108 diagnosed), and precipitation. The horizontal resolution is 0.5° latitude×0.6667° longitude, and
109 the temporal resolution is daily though the daily values are averaged to create monthly means.

110 The stationary wave model is a fully nonlinear baroclinic model with 14 vertical levels on
111 sigma coordinates with R30 truncation in the horizontal (Ting and Yu 1998). The model
112 variables include vorticity, divergence, vertical velocity (sigma coordinate), surface pressure,
113 geopotential height, and temperature. A rigid-lid boundary condition is applied at the top and the
114 surface of the model atmosphere. For damping, Rayleigh friction and Newtonian cooling are
115 applied in the vorticity, divergence, and temperature equations to ensure meaningful solutions.
116 For further details of the model see Ting and Yu (1998).
117
118 **3. Impact of the EA/WR pattern on temperature and precipitation**
119 The leading modes of large-scale teleconnections are computed from the monthly mean
120 upper-level (250hPa) geopotential height field. The climatologies for each month of DJF were
121 first removed from the raw data. A rotated EOF (REOF) technique (Richman 1986) was applied
122 to the resulting anomaly data spanning the past 33-winters. The first four REOFs, in order of
123 decreasing variance, are the NAO (Wallace and Gutzler 1981; Barnston and Livezey 1987), the
124 SCA (Washington et al. 2000; Bueh and Nakamura 2007), the EA (Barnston and Livezey 1987;
125 Bojariu and Reverdin 2002), and the EA/WR (Barnston and Livezey 1987; Washington et al.
126 2000). Please note that a previous study using an alternative rotation method also captured the
127 NAO as the first mode followed by SCA (Hannachi et al. 2009). The eigenvectors (the spatial
128 distributions) are shown in the left panel of Figure 1, with the corresponding principal
129 component (PC) time series shown in the right panel. Note that all spatial patterns and PC time
130 series are plotted for what is conventionally considered to be the positive phase of the pattern.
131 Also shown in the right panel are the teleconnection indices archived at the National Oceanic and
132 Atmospheric Administration (NOAA)/National Center for Environmental Prediction

(NCEP)/Climate Prediction Center (CPC) (ftp://ftp.cpc.ncep.noaa.gov/wd52dg/data/indices/tele_index.nh). The PC time series and the index time series are in good agreement, confirming that the previously identified teleconnection patterns have been successfully captured. This study has examined the sensitivity of the patterns to the domain size (e.g., to include the entire northern hemisphere) and found that the spatial distributions of the REOFs are robust with respect to changes in the domain (figure not shown). Note that an AO (Thompson and Wallace, 1998) mode was captured as the fourth REOF (not shown), though in our regional analysis, the NAO likely already includes some of the variability of the AO.

The EA/WR pattern (REOF 4), the main focus of the present study, has two large-scale anomaly centers located just north of the Caspian Sea and western Europe, influencing Eurasian climates (Figure 1d). During the positive phase of the EA/WR, a negative height anomaly occurs over the Atlantic near 40°W and 40-45°N, while a positive anomaly is found over central Europe (0-30°E). The EA/WR appears to originate in the North Atlantic and extends northeastward across Europe and European Russia (Barnston and Livezey 1987; Washington et al. 2000).

In order to quantify the temperature and precipitation anomalies associated with each teleconnection pattern, and to help explain how those anomalies are produced in different regions, several atmospheric variables at low levels (i.e., near surface and 850hPa) are regressed onto the time series associated with each z250 hPa height PC. In particular, the regressed field ($R_M(x,y)$) for the Mth mode at grid point (x,y) is defined as

$$R_M(x,y) = \sum_{t=1}^{nt} T(x,y,t) \cdot P_M(t), \quad (1)$$

where $T(x,y,t)T(x,y)$ is the anomaly field in question at time step t, and $P_M(t)$ represents the

normalized monthly PC time series of the z250 hPa height for the Mth mode. In the above summation, *nt* is equal to 99 months, the length of the analysis period.

In this study, the advective temperature change arising from the circulation anomaly is calculated as $-V_{Tel} \cdot \nabla T_{Cli}$ (Linkin and Nigam 2008), where V_{Tel} indicates the horizontal winds associated with the EA/WR pattern and T_{Cli} refers to the climatological temperatures (Figure 2c). Note that the contribution from the nonlinear component, $-V_{Tel} \cdot \nabla T_{Tel}$, and the other linear component, $-V_{Cli} \cdot \nabla T_{Tel}$, is by comparison small.

In general, the geographical distribution of the variables in Figure 2 reflects the upper-level height anomaly distribution that has a wave structure spanning the Atlantic, Europe, and western Russia shown in Figure 1 (cf., Barnston and Livezey 1987; Washington et al. 2000). Such a wave structure is expected to be associated with circulation anomalies and temperature advection patterns that produce regions of alternating warm and cold weather. Figure 2b clearly shows a strong anticyclonic circulation over Europe and cyclonic circulation over western Russia in the event of positive EA/WR. These anomaly pattern helps to determine temperature advection characterized by warm advection over the northeast Atlantic extending into western Europe and western Africa (~20°W~10°E), and Russia northeast of the Caspian Sea. Cold advection occurs primarily over eastern Canada, and Russia near the Ural Mountains (Figure 2c), where northerly flow located west of the negative SLP anomaly is dominated.

The resulting temperature anomaly pattern in Figure 2a reflects this spatial distribution of circulation and temperature advection with the strongest response occurring over Russia. Figure 2a reveals that the 2-meter air temperature (T2m) anomalies associated with the EA/WR extend to North America, the Middle East, Africa, and Eurasia. Western Russia shows larger magnitude of T2m anomalies (>1°C) than the magnitude of anomalies over the other regions (Figure 2a).

178 During the positive EA/WR, positive anomalies are found over the eastern US, western Europe,
179 and Russia east of Caspian Sea. Eastern Canada, far eastern Europe including Ural Mountains
180 (~60°E), the Middle East and northeastern Africa regions are characterized by negative
181 anomalies, although the anomalies are not statistically significant at the 10% level over part of
182 the regions.

183 Figure 2d shows that distribution of precipitation anomalies is strongly coupled with the
184 anomalous SLP and lower-level circulation pattern (Figure 2b). The positive precipitation
185 anomalies are clearly found where negative SLP anomalies are located, and the opposite is true
186 for the negative precipitation anomalies. During the positive EA/WR, the mid-latitude Atlantic
187 and the central Russia (~60°N) are the main regions that have the above-average precipitation,
188 while the eastern Canada and European region experience the below-average precipitation. A
189 weak positive precipitation anomaly is observed over the eastern US, but the magnitude is
190 relatively small. The anomalies described in Figure 2 are of course by definition of opposite sign
191 for the negative phase of the EA/WR.

192

193 4. **The Connection with Rossby Waves**

194 *a. Wave activity fluxes*

195 In this section the relationship between the EA/WR teleconnection pattern and large-scale
196 Rossby waves is examined. Wave activity flux (WAF) vectors are calculated to identify the
197 spatial distribution of wave propagation associated with the EA/WR. Following Plumb (1985),
198 the stationary WAF is given as

$$F_s = p\cos\varphi \begin{pmatrix} v'^2 - \dfrac{1}{2\omega\sin\varphi}\dfrac{\partial(v'\Phi')}{\partial\lambda} \\ -u'v' + \dfrac{1}{2\omega a\sin 2\varphi}\dfrac{\partial(u'\Phi')}{\partial\lambda} \\ \dfrac{2\omega\sin\varphi}{S}\left[v'T' - \dfrac{1}{2\omega a\sin 2\varphi}\dfrac{\partial(T'\Phi')}{\partial\lambda}\right] \end{pmatrix}$$

199

200 where the variables (u, v), p, T, and Φ represent the zonal and meridional wind, pressure,
201 temperature, and geopotential height, respectively, and where λ and φ represent longitude and
202 latitude. The constant ω is the earth's rotation rate (=7.292 × 10^{-5} rad s^{-1}) and a is the radius of
203 the earth. The prime denotes the deviation from the zonal mean at each latitude and height.
204 $S = \frac{\partial\hat{T}}{\partial z} + \frac{\kappa\hat{T}}{H}$ is the static stability; the caret indicates an areal average over the Northern
205 Hemisphere; κ (=287 J K^{-1} kg^{-1}/1004 J K^{-1} kg^{-1}) is the ratio of gas constant to specific heat at
206 constant pressure, and H is a constant scale height.

207 Figure 3 shows the horizontal WAF distribution at 300hPa. The pattern suggests that the
208 EA/WR reflects Rossby waves responding to forcing in the mid-latitude Atlantic. Specifically,
209 there is a clear wave train extending across the Atlantic, western Europe and Russia associated
210 with the EA/WR.

211

212 *b. Rossby wave source*

213 The source regions and the propagation characteristics of the EA/WR teleconnection are
214 investigated in this section using the stationary wave model (SWM) of Ting and Yu (1998) (see
215 section 2 for the model description). This study focuses on both diabatic heat forcing and
216 transient vorticity forcing, the importance of which in generating large-scale wave trains in the
217 extratropics has been shown by previous studies (Sardeshmukh and Hoskins 1988; Qin and
218 Robinson 1993). Also, the upper-level WAF pattern (Figure 3) suggests that the Rossby wave

source (RWS) is located over the extratropical Atlantic, in a region where transient eddies associated with the Atlantic storm track could play a role (Bueh and Nakamura 2007). Previous studies emphasize the importance of changes in wintertime extratropical transient eddy activity for forcing changes in upper-level jet intensity and its extension (e.g., Losada et al. 2007).

Following Schubert et al. (2011) this study attempts to reproduce the observed teleconnection patterns by forcing the SWM model with a series of regional heat and vorticity forcing functions, respectively, located at 5° longitude/latitude intervals distributed throughout the North Atlantic. The 3-dimensional basic state for this run is the MERRA climatology computed from the past 33 winters (1979/80-2011/12). The similarity is assessed between the SWM response to each forcing function and the observed teleconnection by calculating their spatial correlation over the North Atlantic and Europe domain (60°W-60°E ,20-80°N). These correlations are then plotted at the forcing locations (Figure 4).

Figure 4a shows that the largest correlations for the SWM response to heat forcing are found over the subtropical western Atlantic near the Caribbean Sea. Correlation values over the mid-latitude Atlantic are generally small. The subtropical region where the largest correlation is found is consistent with the region of the largest positive diabatic heating anomaly (Figure 4b) at mid-troposphere and SST anomaly (Figure 4c) regressed onto the EA/WR, indicating a possible heat source over the region to generate the Rossby-type wave that resembles the EA/WR. This possible positive relationship between SST anomaly over the subtropical western Atlantic and the phase of EA/WR is in good agreement with Wang et al. (2011). The study suggested that cold North Atlantic SST anomalies are associated with the negative EA/WR pattern that enhances the Siberian high and east Asian winter monsoon.

As for the transient vorticity forcing, Figure 5a shows that the EA/WR has spatial correlations greater than 0.7 over the mid-latitude Atlantic basin (~40°W, ~40°N), suggesting they have a substantial Rossby wave component that resembles the EA/WR pattern driven by extratropical transients. It also suggests that this wave pattern is most easily forced in the central North Atlantic near the climatological jet exit region (please see the superimposed contours in Figure 5a). Blackburn and Hoskins (2001) found that the exit region of the Atlantic jet stream was important for cyclone growth and dynamically forced ascent. Distribution of upper-level (250hPa) daily zonal wind variance in Figure 5b shows the largest variance over this mid-latitude North Atlantic, indicating the strongest transient eddy activity around the wave source region.

Figure 6 shows some examples of the SWM response to idealized forcing chosen to resemble the observed EA/WR. The location of the heat forcing and vorticity forcing, respectively, was chosen based on the location of the largest correlation values in Figures 4 and 5 which is 80-70°W, 20-25°N for the heat forcing, and 45-35°W, 35-40°N for the vorticity forcing (Figures 6a,b). The SWM responses (upper-panels) and the observed patterns captured by REOFs (lower-panels) show substantial similarities. In particular, positive heat forcing in the subtropical North Atlantic (20-25°N) and vorticity forcing in the mid-latitude Atlantic (35-40°N), respectively, generates a stationary wave with maximum amplitude over the high latitude North Atlantic, the Scandinavian peninsula, and the Eurasian continent (Figures 6a,b), similar to the observed EA/WR pattern in Figure 6c. The SWM, however, also generates a low latitude response (Figure 6a) that is not found in the observed pattern. Overall, Figure 6 supports the idea that EA/WR pattern is associated with large-scale Rossby wave responses to diabatic heat forcing and vorticity forcing over the extratropical Atlantic.

Next, rather than deducing the RWS based on the SWM responses to idealized forcing, the RWS is estimated directly based on observation data (MERRA data). Following Sardeshmukh and Hoskins (1988) and Qin and Robinson (1993), the RWS is derived from the quasi-geostrophic vorticity equation as

$$\text{RWS} = -V_\chi \cdot \nabla(\zeta + f) - (\zeta + f)\nabla \cdot V_\chi, \quad (1)$$

where V_χ is the divergent (irrotational) wind vector, ζ the relative vorticity, and f the Coriolis parameter. The linearized form of RWS can be written as

$$\text{RWS}_\text{L} = -V_\chi' \cdot \nabla(\bar{\zeta} + \text{f}) - (\bar{\zeta} + \text{f})\nabla \cdot V_\chi' - \zeta' \nabla \cdot \bar{V}_\chi - \bar{V}_\chi \cdot \nabla\zeta', \quad (2)$$

where the overbar denotes the climatological mean and the prime denotes the anomaly associated with the teleconnection pattern (e.g., EA/WR). The first and fourth term on the right hand side of (2) are associated with vorticity advection, whereas the second and third terms involve the generation of wave vorticity by the divergence of the divergent wind (i.e., vorticity stretching). Sardeshmukh and Hoskins (1988) and Qin and Robinson (1993) found that the first and fourth terms capture the main features of the tropical source whereas the second and third terms determine the main features of the extratropical RWS (Seo and Son 2012). Figure 7a shows the distribution of the RWSs characterized by positive peak over the mid-latitude Atlantic. Location of the peak values at 50-30°W and 35-50°N is consistent with the positive spatial correlation maximum shown in Figure 5a.

In order to confirm that the regions forcing the EA/WR wave patterns are indeed in the locations we discussed in Figures 4 through 6, the EA/WR pattern is reproduced with the RWS forcing in the region outlined in Figures 7a. The region is upstream of the EA/WR pattern, and located where the magnitude of spatial correlation between the patterns of observed teleconnection and idealized model result (by transient vorticity forcing) is high (Figure 5a). The

responses to the forcing in those regions (Figure 7b) show a reasonable similarity with the observed EA/WR pattern captured by the REOFs (Figure 6c).

c. Sensitivity to background flow change (NAO and ENSO)

Since variations in the NAO impact the upper-level westerlies over the North Atlantic, this study examines whether the NAO has an impact on the other patterns through NAO-related changes in the base state. Table 1 shows the variance of the PCs of the EA/WR REOFs for different NAO phases. The results show that the variances of the PCs are larger on average in the event of a positive NAO. The dependency of the intensity of the EA/WR pattern upon the NAO phase indicates that strong wind and storminess over the European mainland is more likely to occur during the positive NAO, as suggested by Donat et al. (2010).

In order to more clearly demonstrate that the EA/WR pattern is indeed sensitive to the NAO phase, the SWM response to vorticity sources is re-examined with modified base states. In particular, this examination considers base states that have added to it +/- one standard deviation of the NAO pattern. Additional experiments were conducted by incorporating +/- one standard deviation of the ENSO component[1]. Figure 8 shows the changes made to the base state, with one standard deviation of the positive (negative) NAO (Fig. 8a) acting to accelerate (decelerate) the westerlies between 40-60°N over the Atlantic, and decelerate (accelerate) them between 20-40°N. El Niño also plays a role in displacing the Atlantic storm track and modifying the westerlies, but with smaller magnitude compared with the NAO impact (Figure 8b).

Four SWM experiments were conducted to quantify the impact of the NAO and ENSO on the EA/WR. Figure 9 shows the EA/WR response to the positive NAO (Figure 9a) and negative

[1] Note that the ENSO component is captured as a higher REOF (not shown) occurring just after the EA/WR mode.

NAO (Figure 9b), respectively. The transient vorticity forcing is identical to that referred to in Figure 5. An EA/WR-like pattern is generated for both basic states (Figures 9a,b), though there are differences in the intensities of the ridges/troughs between the two wave patterns. The wave path is also different. In general, EA/WR is better organized and strengthened over the Atlantic and western Europe when the mean state is modified with a positive NAO component. This is, to a great extent, consistent with Wanner et al. (2001) and Scherrer et al. (2006) who found a greater possibility of strong pressure patterns (teleconnection) and atmospheric blocking over the European mainland during the positive phase of the NAO. The wave track is also more realistic with the positive NAO added to the base state (Figure 9a). For the case of the negative NAO, there is a northward displacement of the anomalies making the response less like the observed EA/WR pattern (Figure 9b). Also, the pattern shows relatively smaller amplitude especially over the Atlantic and western Europe. It appears that the stronger upper-level westerly jet at 40-60°N over the Atlantic during the positive NAO may facilitate the eastward propagation of the EA/WR over the European continent. In contrast, the main anomalies during the negative NAO tend to be situated further west over Greenland due to weakened upper-level westerlies between 40-60°N.

The above experiments were repeated for the modified mean states reflecting the ENSO impact. The results show some differences in the EA/WR pattern for the El Niño and La Niña cases, but the differences are considerably less than those for the NAO shown in Figure 9, reflecting the smaller change in the upper-level jet compared to that associated with the NAO (figure not shown). This suggests that a very strong ENSO is necessary to noticeably modulate the EA/WR patterns, and that in general the NAO is a greater factor in modulating those patterns.

5. Concluding remarks

331 This study has investigated the EA/WR, the important winter atmospheric teleconnection
332 pattern generated over the North Atlantic region. The focus is on providing further insights into
333 the spatial scope and physical mechanisms of the impacts, as well as the dynamical mechanisms
334 responsible for the existence of EA/WR.

335 It was found that the four leading REOFs of the upper tropospheric height field consist of, in
336 order of decreasing variance, the NAO, the SCA, the EA, and the EA/WR. There have been few
337 studies that have examined in any detail the impact of the EA/WR on regional temperatures and
338 precipitation across Eurasia. Here the present study found that the positive (negative) EA/WR is
339 associated with a strong warming (cooling) over Russia east of the Caspian Sea whereas it is
340 associated with cooling (warming) over the Ural Mountains of northern Russia. The strong
341 temperature response over those regions is linked to a surface pressure anomaly near the Ural
342 Mountains and associated strong atmospheric circulation and thermal advection anomalies. Other
343 impacts linked to the positive (negative) phase of the EA/WR are a warming (cooling) over the
344 eastern US and western Europe, and a cooling (warming) over eastern Canada, far eastern
345 Europe and the Middle East, though these tend to be weak. It was also found in this study that
346 precipitation anomalies are strongly coupled with the anomalous SLP and lower-level circulation
347 pattern. Positive (negative) precipitation anomalies are pronounced over the mid-latitude Atlantic
348 and the central Russia (~60°N), while the negative (positive) anomalies are mainly distributed
349 over the eastern Canada and European region during the positive (negative) EA/WR. The eastern
350 US region exhibits the positive (negative) anomalies, but the magnitudes are generally small
351 during the positive (negative) phase of the EA/WR.

352 The second part of this study examined the relationship of the EA/WR teleconnection to
353 large-scale Rossby waves. It was found, using a SWM, that the EA/WR pattern could be

reproduced by forcing the model with vorticity transients over the mid-latitude North Atlantic (35-40°N) and with diabatic heating over the subtropical western Atlantic (15-20°N). The results appear consistent with Bueh and Nakamura (2007) in that the transient eddies migrating along the Atlantic storm track play an important role for emanation of the Rossby waves from the mid-latitude Atlantic. The RWS calculation based on observation provides supporting evidence that the RWS regions over the Atlantic are at ~40°W and ~40°N for the EA/WR. It was further shown that it is the vorticity transients near the Atlantic jet region (~40°N, ~40°W) that are important for generating the EA/WR-like response.

This study found that the EA/WR-like Rossby wave responses in the SWM show some sensitivity to the base state, with better-organized eastward propagation and enhanced ridge/trough anomalies over the North Atlantic and far western Europe occurring when the base state includes a positive NAO component. This appears to be due to the enhancement of the upper-level westerlies (40-60°N) associated with the positive NAO. Less organized EA/WR pattern is simulated when the base state includes a negative NAO component. This finding appears to support the argument by earlier studies (Pavan et al. 2000; Wanner et al. 2001: Scherrer et al. 2006) that addressed weaker pressure patterns and associated blocking over the European continent during the negative NAO.

The modulation of the EA/WR pattern by other key large-scale modes of varaibility such as ENSO was also examined. The modulation of the teleconnection patterns by ENSO (El Niño versus La Niña) is less pronounced compared with the NAO impact, suggesting a greater role of NAO in modulating those teleconnection patterns. The result emphasizes the importance of upper-level westerly wind changes over the North Atlantic in modulating these teleconnection

patterns, suggesting that the variability in these regions consists of a complex interplay of the leading patterns.

This study provides fundamental assessment of the EA/WR pattern in terms of 1) its climate impact on surface temperature and precipitation over vast area across North America, North Africa and Europe including western Russia, and 2) relation of the EA/WR to Rossby wave propagation. Investigation of the EA/WR should further be complemented by more detailed studies, including predictability of the generation of EA/WR pattern. Better identification of extra-tropical heating (or cooling) over the western subtropical Atlantic and upper-level transient eddy activity near the mid-latitude central Atlantic should be a key factor for reliable prediction of the EA/WR pattern.

387 References

388 Barnston AG, Livezey RE (1987) Classification, seasonality and persistence of low-frequency
389 atmospheric circulation pattern. Mon Weather Rev 115: 1083-1126

390 Blackburn M, Hoskins BJ (2001) The UK record-breaking wet autumn 2000. pp. 38–40 in UK
391 Universities Global Atmospheric Modelling Programme, UGAMP Newsletter 24. Available
392 from Meteorological Department, University of Reading, UK.

393 Bojariu R, Reverdin G (2002) Large-scale variability modes of freshwater flux and precipitation
394 over the Atlantic. Clim Dyn 18: 369-381 DOI:10.1007/s003820100182

395 Bueh C, Nakamura H (2007) Scandinavian pattern and its climate impact. Quart J Royal Meteor
396 Sci 133: 2117-2131

397 Donat MG, Leckebusch GC, Pinto JG, Ulbrich U (2010) Examination of wind storms over
398 Central Europe with respect to circulation weather types and NAO phases. Int J Climatol
399 30: 1289-1300

400 Hannachi A, Unkel S, Trendafilov NT, Jollife IT (2009) Independent component analysis of
401 climate data: A new look at EOF rotation. J Clim 22: 2797-2812

402 Hurrell JW (1995) Decadal trends in the North Atlantic Oscillation: Regional temperatures and
403 precipitation. Science 269: 676-679

404 Kim YJ, Kim KY, Jhun JG (2013) Seasonal evolution mechanism of the East Asian winter
405 monsoon and its interannual variability. Clim Dyn 41: 1213-1228

406 Lim YK, Kim HD (2013) Impact of the dominant large-scale teleconnections on winter
407 temperature variability over East Asia. J Geophys Res 118: 7835-7848
408 doi:10.1002/jgrd.50462

409 Linkin ME, Nigam S (2008) The North Pacific Oscillation-West Pacific teleconnection pattern:
410 Mature-phase structure and winter impacts. J Clim 21: 1979-1997
411 Losada T, Rodriguez-Fonseca B, Mechoso CR, Ma HY (2007) Impact of SST anomalies on the
412 North Atlantic atmospheric circulation: a case study for the northern winter 1995/1996.
413 Clim Dyn 29: 807-819
414 Pavan V, Tibaldi S, Brankovic C (2000) Seasonal prediction of blocking frequency: Results from
415 winter ensemble experiments. Quart J Roy Meteor Soc 126: 2125-2142
416 Plumb RA (1985) On the three-dimensional propagation of stationary waves. J Atmos Sci 42:
417 217-229
418 Qin J, Robinson WA (1993) On the Rossby wave source and the steady linear response to
419 tropical forcing. J Atmos Sci 50: 1819-1823
420 Richman MB (1986) Rotation of principal components. J Climatol 6: 293–335
421 Rienecker MM, et al. (2011) MERRA – NASA's Modern-Era Retrospective Analysis for
422 Research Applications. J Clim 24: 3624-3648
423 Sardeshmukh PD, Hoskins BJ (1988) The generation of global rotational flow by steady
424 idealized tropical divergence. J Atmos Sci 45: 1228-1251
425 Shabbar A, Huang J, Higuchi K (2001) The relationship between the wintertime North Atlantic
426 Oscillation and blocking episodes in the North Atlantic. Int J Climatol 21: 355-369
427 Scherrer SC, Croci-Maspoli M, Schwierz C, Appenzeller C (2006) Two-dimensional indices of
428 atmospheric blocking and their statistical relationship with winter climate patterns in the
429 Euro-Atlantic region. Int J Climatol 26: 233-249

Schubert SD, Wang H, Suarez M (2011) Warm season subseasonal variability and climate extremes in the Northern hemisphere: The role of stationary Rossby waves. J Clim 24: 4773-4792

Seo KH, Son SW (2012) The global atmospheric circulation response to tropical diabatic heating associated with the Madden-Julian Oscillation during northern winter. J Atmos Sci 69: 79-96

Sugimoto S, Hanawa K (2010) The wintertime wind stress curl field in the North Atlantic and its relation to atmospheric teleconnection patterns. J Atmos Sci 67: 1687-1694

Thompson DWJ, Wallace JM (1998) The Arctic oscillation signature in the wintertime geopotential height and temperature fields. Geophys Res Lett 25(9): 1297-1300 doi:10.1029/98GL00950

Ting M, Yu L (1998) Steady response to tropical heating in wavy linear and nonlinear baroclinic models. J Atmos Sci 55: 3565-3582

Walter K, Luksch U, Fraedrich K (2001) A response climatology of idealized midlatitude thermal forcing experiments with and without a storm track. J. Clim 14: 467–484.

Wallace JM, Gutzler DS (1981) Teleconnections in the geopotential height field during the Northern Hemisphere winter. Mon Weather Rev 109: 784–812

Wang X, Wang C, Zhou W, Wang D, Song J (2011) Teleconnected influence of North Atlantic sea surface temperature on the El Niño onset. Clim Dyn 37: 663-676 DOI:10.1007/s00382-010-0833-z

Wanner H, Brönnimann S, Casty C, Gyalistras D, Luterbacher J, Schmutz C, Stephenson DB, Xoplaki E (2001) North Atlantic Oscillation – concepts and studies. Surveys in Geophys 22: 321-382

453 Washington R, Hodson A, Isaksson E, Macdonald O (2000) Northern hemisphere teleconnection
454 indices and the mass balance of Svalbard glaciers. Int J Climatol 20: 473-487

455 Table 1 Variance of the principal components for EA/WR with respect to the phase of
456 NAO. Numeric range in each cell represents the 90% confidence interval .

	EA/WR
NAO (+) (17 yrs)	1.28 0.57~2.00
NAO (–) (15 yrs)	0.72 0.30~1.14

457

458

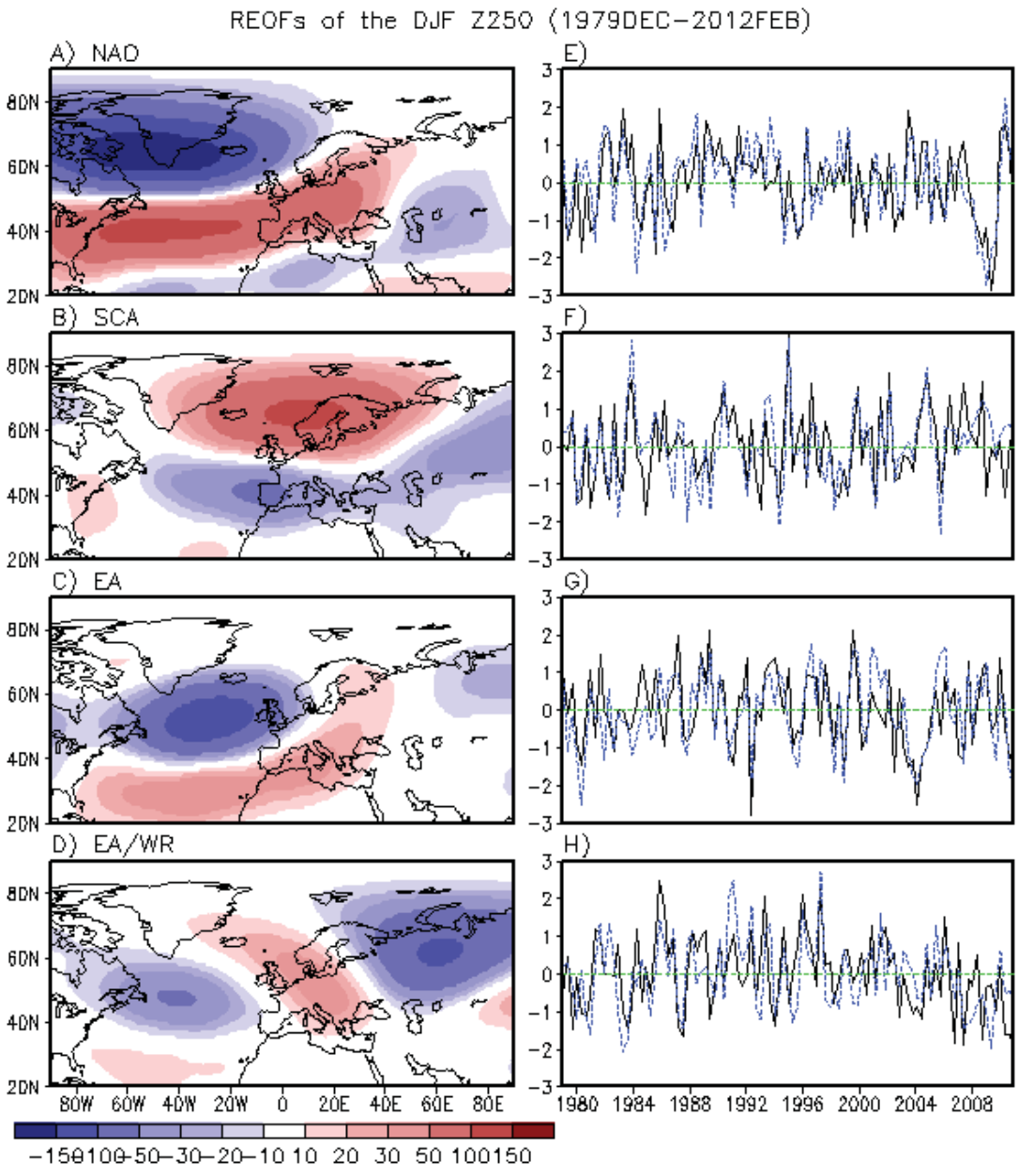

Figure 1. The first four rotated empirical orthogonal functions (REOFs) of the monthly 250hPa height archived from MERRA reanalysis. The data set consists of data for 33 winters from 1979/80 DJF through 2011/12 DJF. The left panel represents the distribution of non-normalized eigenvectors whereas the right panel the corresponding PC represents the time series (solid line). Dashed lines denote the teleconnection pattern indices time series archived at NOAA/NCEP/CPC.

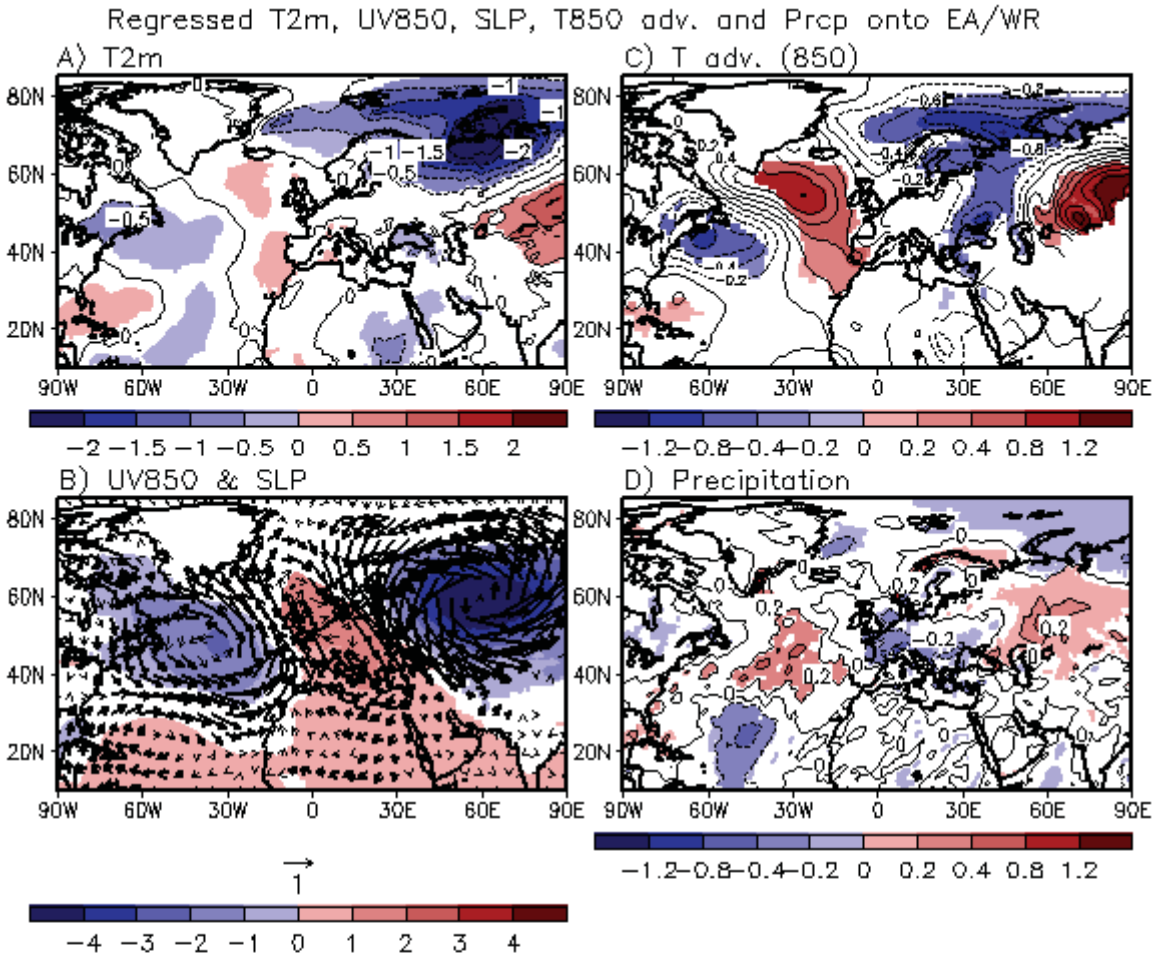

Figure 2. Distribution of a) 2 meter air temperature anomalies, b) sea level pressure and 850hPa circulation, c) the advective temperature change ($-V_{Tel} \cdot \nabla T_{Cli}$) by 850hPa atmospheric circulation, and d) precipitation associated with 1 standard deviation in the positive EA/WR PC based on a linear regression. For the calculation of temperature advection, V_{Tel} denotes the horizontal winds regressed onto EA/WR and T_{Cli} represents the climatological temperatures. Shaded are the regions where the anomaly values are statistically significant at 10%. Wind vectors statistically significant at 10% level are plotted thick.

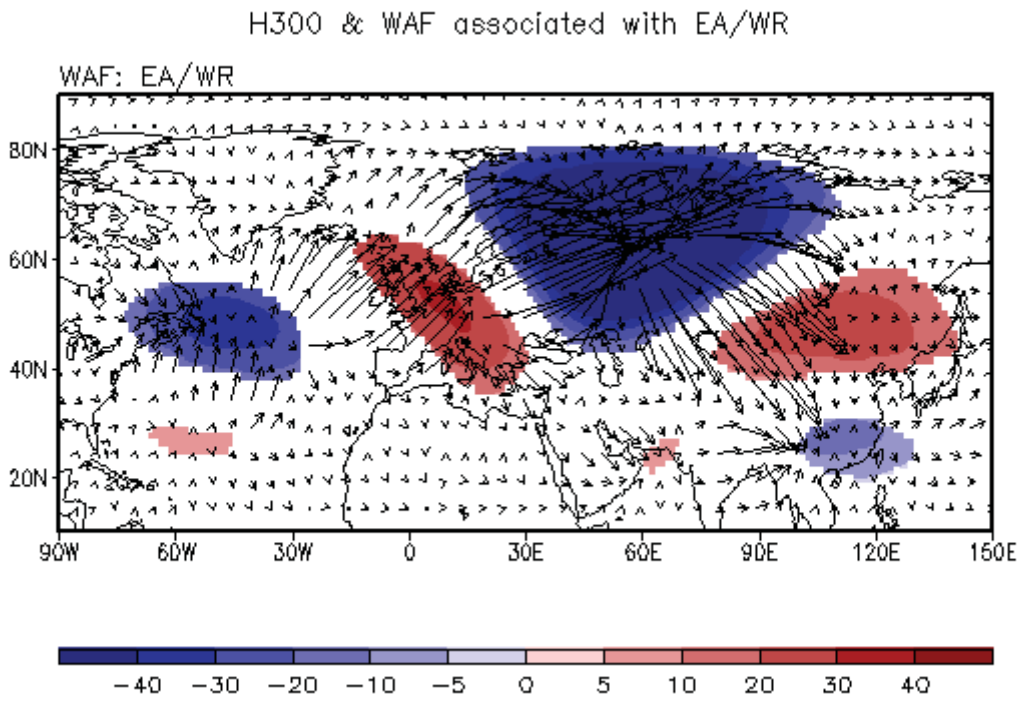

Figure 3. Distribution of the wave activity fluxes and geopotential height anomalies at 300hPa associated with the positive phase of EA/WR. Geopotential height anomalies statistically significant at 10% level are shaded.

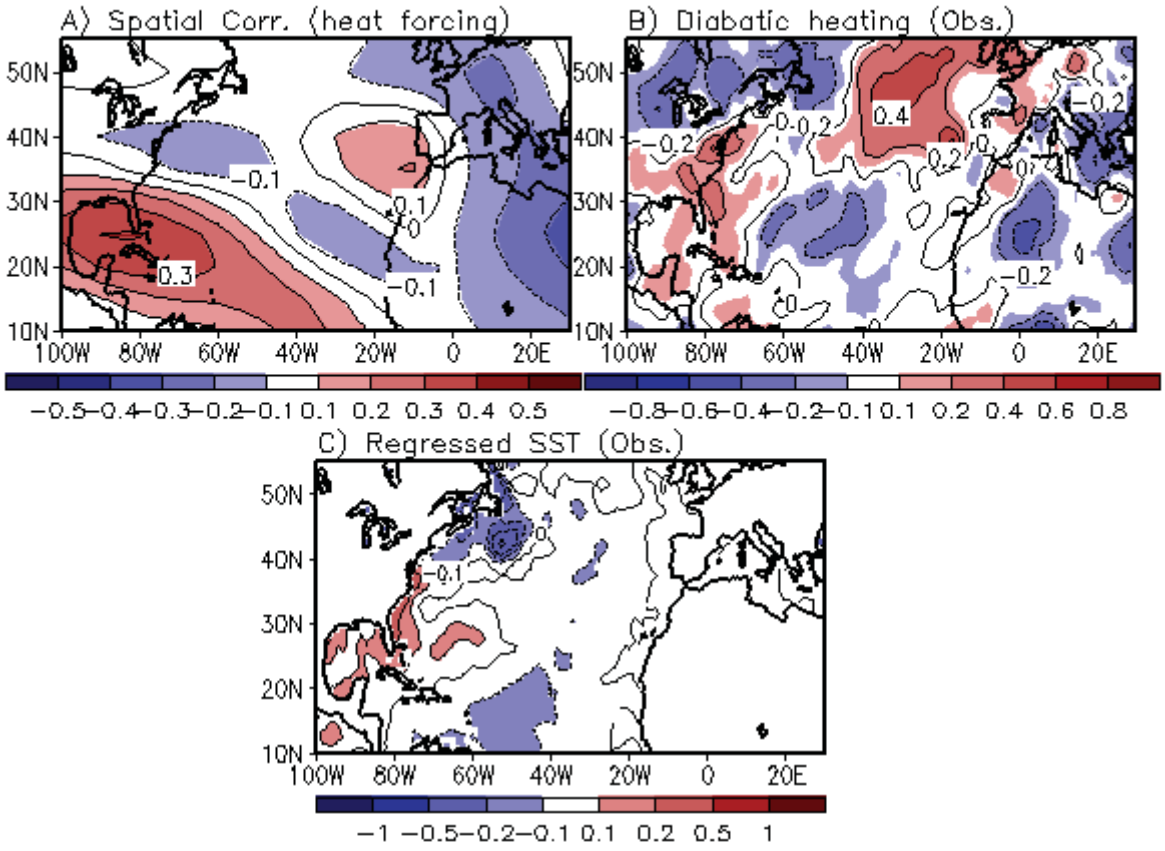

Figure 4. a) Spatial correlations between the observational teleconnection pattern captured by REOF and stationary wave propagation pattern produced by the stationary wave model. The 3-dimensional basic state in the SWM is the MERRA climatology computed from the past 33 winters (1979/80-2011/12). In order to generate the stationary wave at each grid point, diabatic heat forcings with the maximum at mid-troposphere are given, respectively, at the grid points with 5-degree longitude-latitude interval over the Atlantic. Geographical domain for spatial correlation calculation is 60°W~60°E and 20°N~80°N. Correlation values are plotted on the grid points where the diabatic heat forcing is given for generating the stationary wave in the model. b) represents the observed distribution of residually diagnosed diabatic heating anomalies at mid-troposphere (700-300hPa) regressed onto the EA/WR. c) represents the distribution of SST anomalies regressed onto the EA/WR.

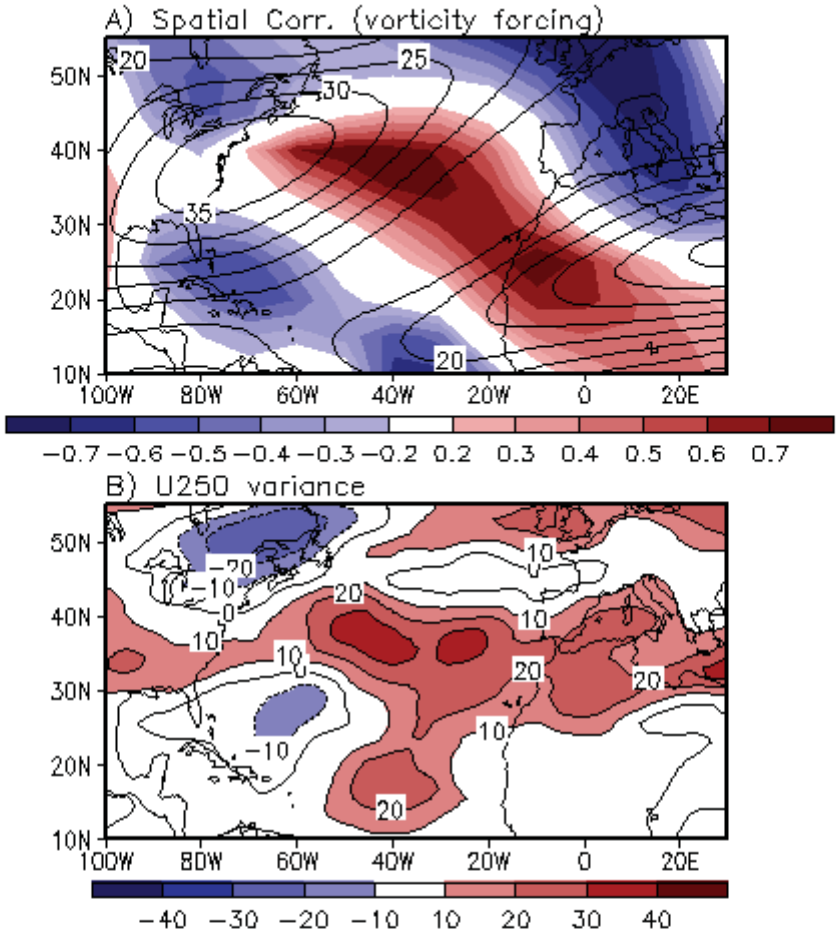

Figure 5. a) Same as Figure 4a except that transient eddy forcings of vorticities are given, respectively, at the grid points with 5-degree longitude-latitude interval over the Atlantic. Correlation values are plotted on the grid points where the transient eddy forcing of vorticity is given for generating the stationary wave in the model. Contours in a) denote the climatological upper-level (300hPa) westerlies. b) represents the distribution of upper-level (250hPa) zonal wind variance regressed onto the EA/WR.

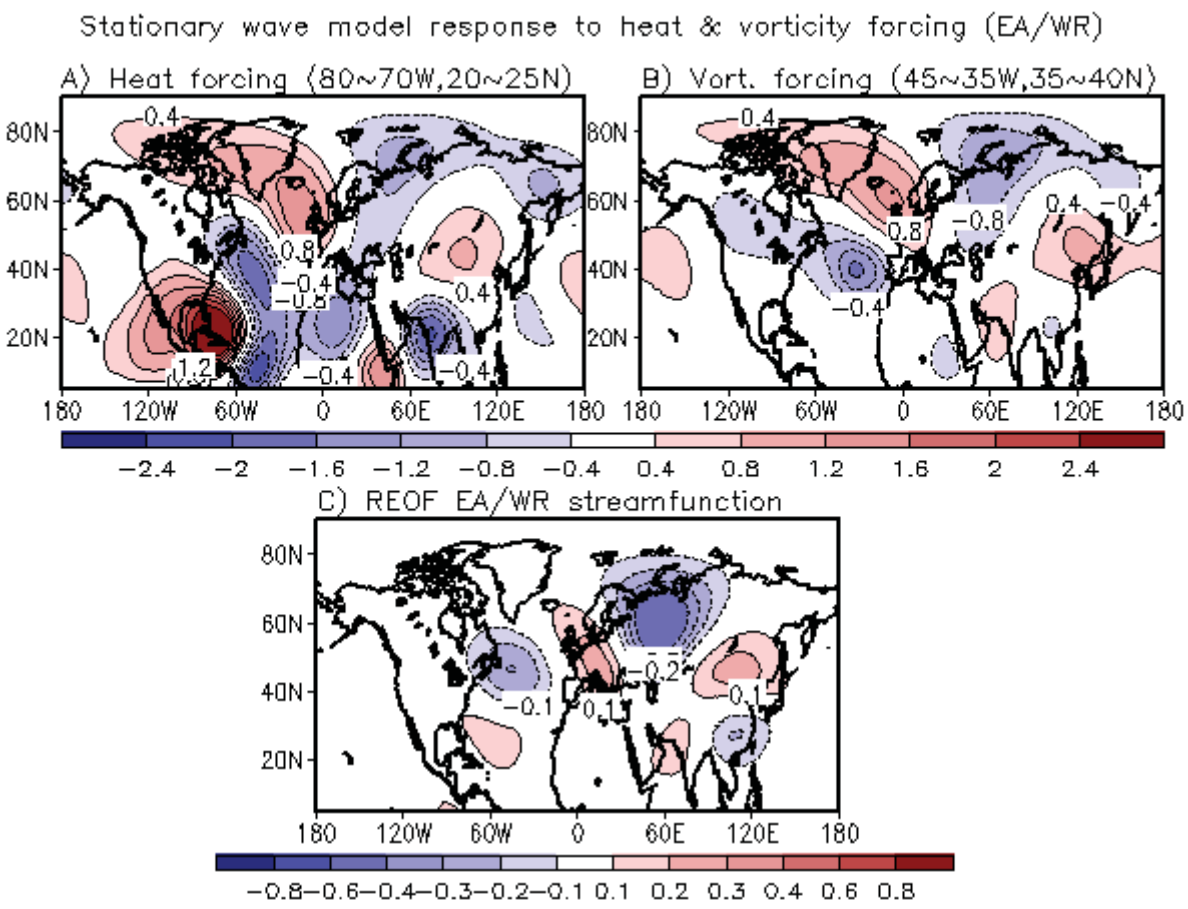

Figure 6. Upper panel: Streamfunction (divided by 10^6) of the simulated large-scale stationary wave propagation (a and b) similar to EA/WR pattern. a) represents the wave propagation forced by diabatic heat source, while b) by transient vorticity forcing. Geographical location of the forcing given in the model is 80~70°W, 25~25°N for the diabatic heat forcing, and 45~35°W, 35~40°N for the transient vorticity forcing, respectively. The 3-dimensional basic state in the SWM is the MERRA climatology computed from the past 33 winters (1979/80-2011/12). Lower panel: Observational teleconnection patterns for c) EA/WR obtained from REOF.

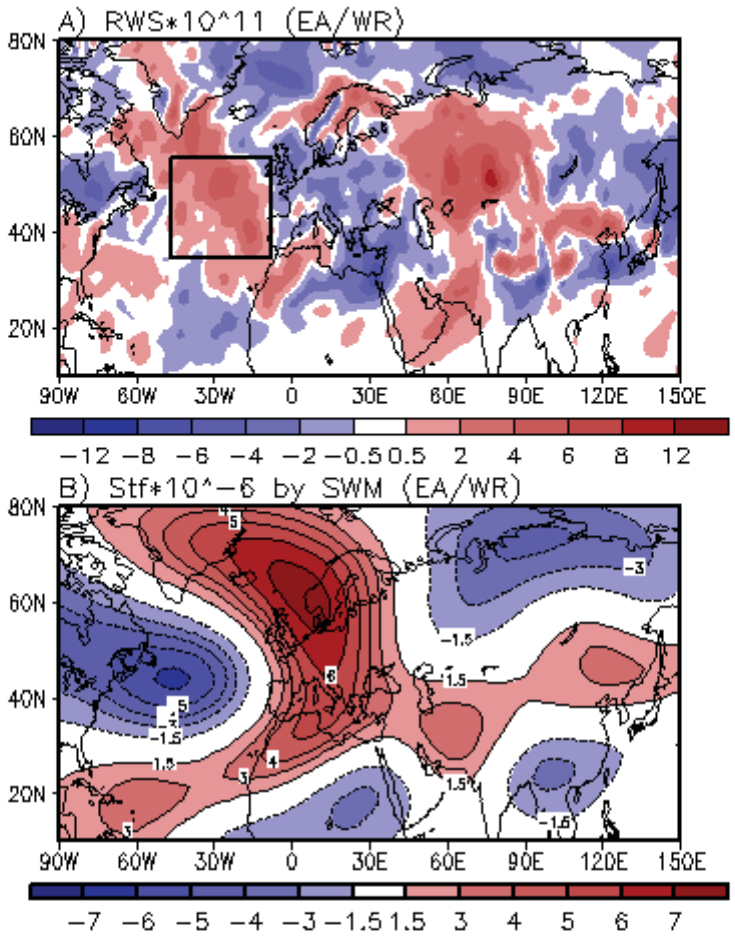

Figure 7. Upper panel: Rossby wave source (RWS) distribution of the observational large-scale stationary wave associated with EA/WR pattern. Source region is represented by positive values (red shading). Lower panel: The EA/WR-like teleconnection patterns reproduced by stationary wave model with the given RWS in the boxed regions shown in upper-panel. Boxed region is where magnitudes of spatial correlations found in Figure 5a are predominantly high.

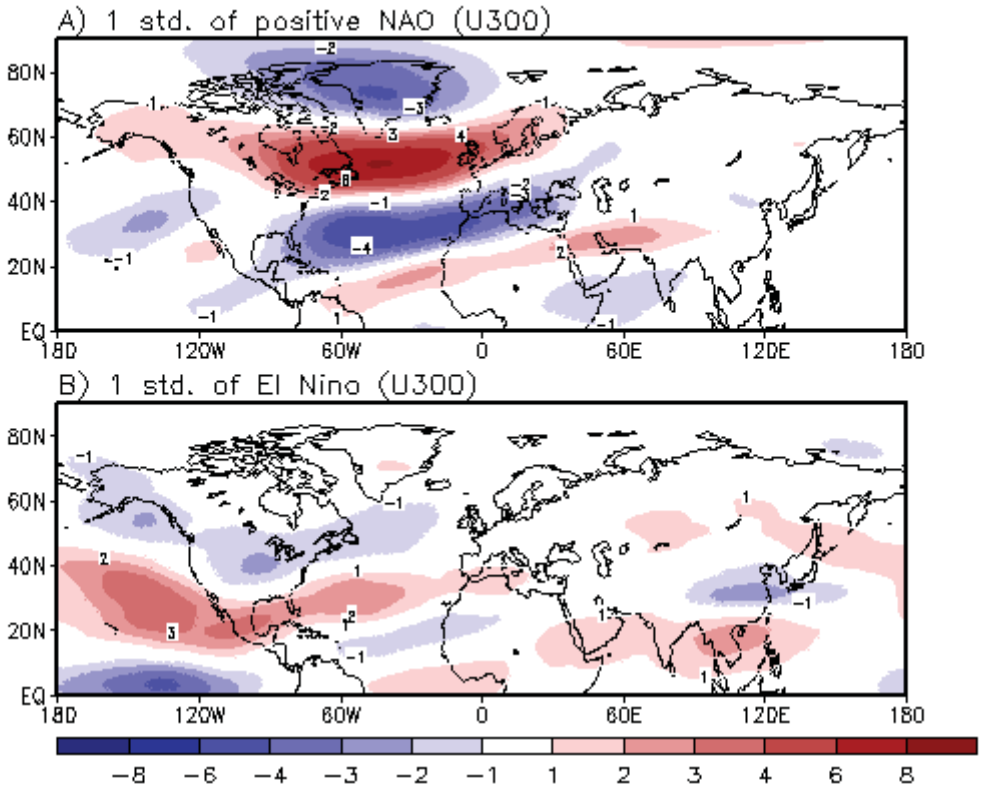

Figure 8. Upper panel (a): Distribution of one standard deviation of the positive NAO component in terms of upper-level (300hPa) westerly. Note that the climatology is the average of the upper-level westerlies over 1979/80-2011/12 DJF period. Lower panel (b): Same as a) but for the positive ENSO (i.e., El Niño) component

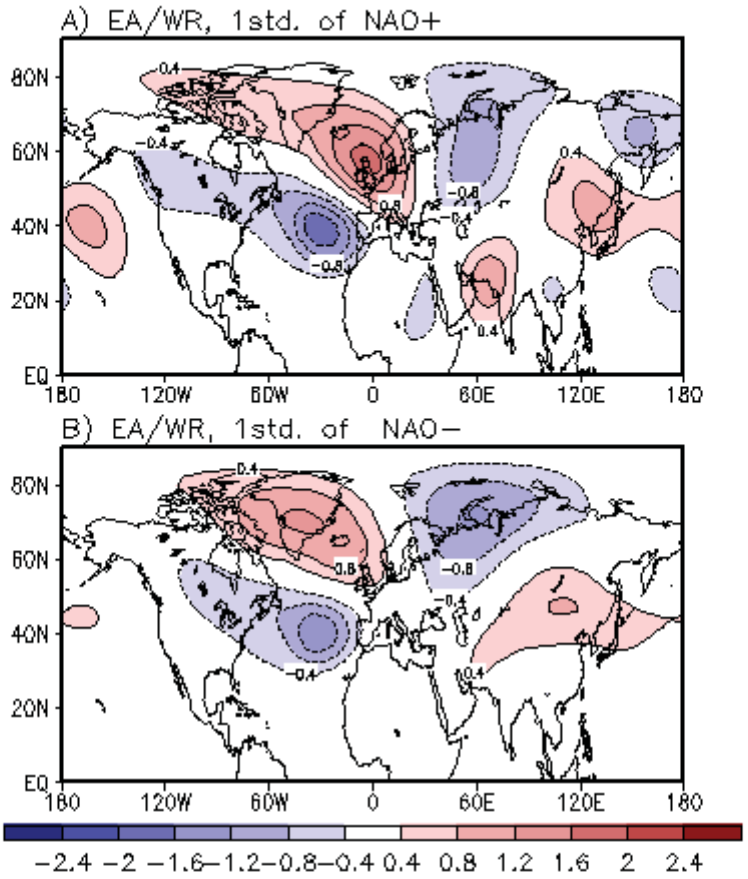

Figure 9. Simulated EA/WR-like Rossby wave train embedded in the modified climatological basis state where one standard deviation of a) positive NAO is added and b) negative NAO is added. Wave propagation patterns are plotted in terms of streamfunction (divided by 10^6).